Dalton Transactions

RSC Publishing

PAPER

View Article Online
View Journal | View Issue

$Ce_4Ag_3Ge_4O_{0.5}$ – chains of oxygen-centered $[OCe_2Ce_{2/2}]$ tetrahedra embedded in a $[CeAg_3Ge_4]$ intermetallic matrix

Cite this: *Dalton Trans.*, 2013, **42**, 15207

Gunter Heymann,[a] Jan F. Riecken,[b] Dirk Johrendt,[c] Sudhindra Rayaprol,[b] Rainer Pöttgen[b] and Hubert Huppertz*[a]

Received 24th June 2013,
Accepted 27th August 2013

DOI: 10.1039/c3dt51683k

www.rsc.org/dalton

The oxidation of an intermetallic phase under high-pressure/high-temperature conditions led to the synthesis of $Ce_4Ag_3Ge_4O_{0.5}$ exhibiting $[OCe_2Ce_{2/2}]$ tetrahedral chains, in which the oxygen atoms statistically occupy the tetrahedral centres. Starting from a 1 : 1 : 1 CeAgGe precursor (NdPtSb type), a multianvil high-pressure/high-temperature experiment at 11.5 GPa and 1250–1300 °C revealed $Ce_4Ag_3Ge_4O_{0.5}$, crystallizing in the space group *Pnma* with the following lattice parameters: a = 2087.3(4), b = 439.9(1), and c = 1113.8(2) pm. Magnetic measurements showed Curie–Weiss behavior above 100 K with an experimental magnetic moment of 2.42 μ_B per Ce atom, close to the value for the free Ce^{3+} ion, clearly indicating trivalent cerium in $Ce_4Ag_3Ge_4O_{0.5}$. Full potential GGA+U band structure calculations resulted in metallic properties and a magnetic ground state with one unpaired 4*f*-electron per cerium in agreement with the experiments.

Published on 12 September 2013.

Introduction

In contrast to the large variety of intermetallic compounds prepared under ambient pressure conditions, the number of high-pressure intermetallics is very low. The investigations are mostly limited to binary systems, presenting a series of new insights into the chemical bonding and electronic effects of high-pressure application.[1] With the successful high-pressure synthesis of the stannides HP-REPtSn (RE = La, Ce, Pr, Nd, Sm) and HP-CePdSn, we recently extended the research into the area of ternary systems.[2–5] Now, we report the first example of an oxidation of an intermetallic phase under high-pressure/high-temperature conditions, leading to a new germanide oxide with the composition $Ce_4Ag_3Ge_4O_{0.5}$.

The oxidation of intermetallic phases to metal oxides under ambient pressure conditions is well known from the research of Hoppe, Yvon, Schuster, and Jung.[6–14] But only a few intermetallic oxides were established, in which crystal structure considerations and chemical analysis revealed the presence of significant oxygen concentrations. For example, the phases $RE_{12}Fe_{32}O_x$ with $x \leq 2$ (RE = Y, Gd, Tb, Dy, Ho, and Er)[15] and Zr_3NiO[16] represent oxygen-stabilized transition metal intermetallic compounds with octahedrally coordinated oxygen atoms. Furthermore, several Nowotny phases of $D8_8$ type structure were stabilized by the presence of small amounts of carbon, boron, oxygen, or nitrogen.[17–19] While the former mentioned phases were synthesized under ambient pressure conditions, the germanide oxide $Ce_4Ag_3Ge_4O_{0.5}$ was synthesized under high-pressure/high-temperature conditions, starting from NdPtSb type CeAgGe[20–22] as a precursor compound. Since elemental silver has been detected in the X-ray powder diagram of the reaction product, the following reaction scheme under the conditions of 11.5 GPa and 1300 °C can be formulated:

$$4\ \mathrm{CeAgGe} + \frac{1}{4}\mathrm{O_2} \rightarrow \mathrm{Ce_4Ag_3Ge_4O_{0.5}} + \mathrm{Ag}.$$

The amount of oxygen needed derives from diffusion, leaking out of the experimental surroundings (oxygen containing ceramics) at temperatures exceeding 1200 °C and from surface oxidation of the milled precursor.

Thus, the structure of $Ce_4Ag_3Ge_4O_{0.5}$ nicely extends the crystal chemistry of the large family of pnictide oxides.[23,24]

[a]*Institut für Allgemeine, Anorganische und Theoretische Chemie, Leopold-Franzens-Universität Innsbruck, Innrain 80-82, A-6020 Innsbruck, Austria. E-mail: Hubert.Huppertz@uibk.ac.at; Fax: +43 (0)512 507-57099; Tel: +43 (0)512 507-57000*

[b]*Institut für Anorganische und Analytische Chemie, WWU Münster, Corrensstraße 30, D-48149 Münster, Germany. E-mail: pottgen@uni-muenster.de; Fax: +49 (0)251 83-36002; Tel: +49 (0)251 83-36001*

[c]*Department Chemie, Ludwig-Maximilians-Universität München, Butenandtstrasse 5-13 (Haus D), D-81377 München, Germany. E-mail: dirk.johrendt@cup.uni-muenchen.de; Fax: +49 (0)89 2180-77431; Tel: +49 (0)89 2180-77430*

Published on 12 September 2013.

Experimental

Synthesis

Starting materials for the synthesis of the CeAgGe precursor were ingots of the rare earth metal (Treibacher, 99.8%), silver wire (Degussa-Hüls, 99.9%), and a germanium bar (Wacker, 99.9%). Details of the precursor preparation can be found in the original work.[22]

The high-pressure/high-temperature synthesis of the new compound $Ce_4Ag_3Ge_4O_{0.5}$ took place *via* a multianvil Walker type module. Carefully milled CeAgGe powder was filled into a boron nitride crucible of the high-pressure assembly. A precast MgO octahedron (Ceramic Substrates & Components, Isle of Wight, UK) with an edge length of 14 mm was used as a pressure medium. Eight tungsten carbide cubes (TSM 10, Ceratizit, Austria) with a truncation of 8 mm, separated by pyrophyllite gaskets, compressed the octahedron (14/8 assembly). Details of the technique for the construction of the different assemblies can be found in ref. 25.

The intermetallic precursor was compressed to a pressure of 11.5 GPa in 3.5 hours and heated to 1250–1300 °C in the following 10 min. After maintaining this temperature for 10 min, the sample was cooled down to 900 °C in 1 min. To enhance the crystallinity of the sample, an annealing period of five hours followed, accompanied by a slow decrease of the temperature from 900 to 700 °C. Afterwards, the sample was cooled down to room temperature within 1 min. After decompression (10.5 hours), the recovered experimental octahedron was broken apart and the sample was carefully separated from the surrounding boron nitride.

The polycrystalline sample of $Ce_4Ag_3Ge_4O_{0.5}$ is silvery with metallic luster and is stable in moist air over weeks. Powdered samples are dark grey. As a by-product during the various syntheses of $Ce_4Ag_3Ge_4O_{0.5}$ we observed a few times the phase $Ce_3Ag_4Ge_4$. Precise structural data of this phase derived from single crystal structure determination are also presented in this paper.

Several phases seem to be stable in a small area of the ternary phase diagram. A third compound with a 1 : 2 : 2 stoichiometric ratio appeared occasionally in this system. The formation of this phase was generally observed at the lower pressure range from 7.5 GPa to 11.5 GPa and was always accompanied by the formation of $Ce_3Ag_4Ge_4$. Experiments without annealing period revealed traces of the starting material CeAgGe. The herein presented phase $Ce_4Ag_3Ge_4O_{0.5}$ was also synthesized at pressures up to 13.5 GPa. Synthesis temperatures may vary from 1100 to 1300 °C resulting in different degrees of crystallinity of $Ce_4Ag_3Ge_4O_{0.5}$.

X-ray crystallography

Intensity data of suitable crystals of $Ce_4Ag_3Ge_4O_{0.5}$ and $Ce_3Ag_4Ge_4$ were collected at room temperature on an Enraf-Nonius Kappa CCD diffractometer (Bruker AXS/Nonius, Karlsruhe) with MoKα-radiation (λ = 71.073 pm) equipped with a rotating anode. Structure solution and parameter refinement (full-matrix least squares against F^2) were successfully performed using the SHELX-97 software suite.[26–29] An absorption correction based on multi-scans[30] was applied to the data set. To check for the deviations from the ideal compositions, the occupancy parameters were refined in separate series of least-squares cycles. All relevant crystallographic data and details of the data collections are listed in Tables 1–4.

Further details of the single crystal structure determination may be obtained from the Fachinformationszentrum

Table 1 Crystallographic data and structure refinements of $Ce_4Ag_3Ge_4O_{0.5}$ and $Ce_3Ag_4Ge_4$

Composition	$Ce_4Ag_3Ge_4O_{0.5}$	$Ce_3Ag_4Ge_4$
M_W	1182.5	1142.2
Crystal system	Orthorhombic	Orthorhombic
Space group	*Pnma*	*Immm*
Radiation	MoKα (λ = 71.073 pm)	MoKα (λ = 71.073 pm)
a/pm	2087.3(4)	1480.62(7)
b/pm	439.9(1)	713.36(6)
c/pm	1113.8(2)	446.74(9)
V/nm^3	1.0228(3)	0.472(1)
Z	4	2
T/K	293(2)	293(2)
D_{calc}/g cm^{-3}	7.68	8.04
Crystal size/mm^3	0.02 × 0.02 × 0.02	0.02 × 0.03 × 0.03
μ/mm^{-1}	34.50	34.70
θ range/°	3° < θ < 32°	3° < θ < 27.5°
Reflections collected	3459	527
Independent reflections [R_{int}]	1986 [0.0303]	330 [0.0192]
Reflections with $I > 2\sigma(I)$	1503	306
Data/parameters	1986/75	330/23
Absorption correction	Multi-scan[28]	Multi-scan[28]
GOF	1.045	1.149
R indices ($I > 2\sigma(I)$)	R_1 = 0.0270 wR_2 = 0.0430	R_1 = 0.0202 wR_2 = 0.0417
R indices (all data)	R_1 = 0.0470 wR_2 = 0.0467	R_1 = 0.0236 wR_2 = 0.0430
Extinction coefficient	0.00012(2)	0.0005(1)
Larg. diff. peak and hole (e Å^{-3})	2.36/−2.11	1.4/−1.1

Table 2 Atomic coordinates and isotropic displacement parameters (pm^2) for $Ce_4Ag_3Ge_4O_{0.5}$ and $Ce_3Ag_4Ge_4$. U_{eq} is defined as one-third of the trace of the orthogonalized U_{ij} tensor. The 4*c* oxygen site is only half occupied

Atom	Wyckoff site	x	y	z	U_{eq}
$Ce_4Ag_3Ge_4O_{0.5}$					
Ce1	4*c*	0.21375(2)	1/4	0.45848(3)	0.0098(1)
Ce2	4*c*	0.03195(2)	1/4	0.37003(3)	0.0102(1)
Ce3	4*c*	0.39643(2)	1/4	0.36594(3)	0.0101(1)
Ce4	4*c*	0.84974(2)	1/4	0.79251(3)	0.0115(1)
Ge1	4*c*	0.71052(3)	1/4	0.70192(6)	0.0106(2)
Ge1	4*c*	0.67748(3)	1/4	0.48522(6)	0.0105(2)
Ge3	4*c*	0.49712(4)	1/4	0.67924(6)	0.0106(2)
Ge4	4*c*	0.39204(4)	1/4	0.01736(7)	0.0144(2)
Ag1	4*c*	0.59572(3)	1/4	0.84665(5)	0.0152(1)
Ag2	4*c*	0.28068(3)	1/4	0.17013(5)	0.0152(1)
Ag3	4*c*	0.54582(3)	1/4	0.44184(5)	0.0142(1)
O	4*c*	0.1390(5)	1/4	0.2983(9)	0.024(4)
$Ce_3Ag_4Ge_4$					
Ce1	2*d*	1/2	0	1/2	0.0091(2)
Ce2	4*e*	0.12981(4)	0	0	0.0094(2)
Ag	8*n*	0.33253(4)	0.19323(8)	0	0.0148(2)
Ge1	4*f*	0.21632(7)	1/2	0	0.0124(3)
Ge2	4*h*	0	0.18010(5)	1/2	0.0102(3)

This journal is © The Royal Society of Chemistry 2013

Published on 12 September 2013.

Karlsruhe, 76344 Eggenstein Leopoldshafen, Germany (Fax: (+49)7247-808-666; e-mail: crysdata@fiz-karlsruhe.de), quoting the depository numbers CSD-417492 ($Ce_4Ag_3Ge_4O_{0.5}$) and CSD-417491 ($Ce_3Ag_4Ge_4$).

Temperature dependent X-ray powder diffraction

The investigation was carried out on a STOE Stadi P powder diffractometer (Mo-Kα_1, λ = 70.93 pm) with a computer controlled STOE furnace: the sample was enclosed in an argon filled quartz capillary and heated from room temperature to 500 °C in 100 °C steps and from 500 °C to 1100 °C in 50 °C steps. Afterwards the sample was cooled down to 500 °C in 50 °C steps, and below 500 °C in 100 °C steps. At each temperature, a diffraction pattern was recorded over the angular range $12.5° \leq 2\theta \leq 21°$.

Magnetic measurements

The magnetic susceptibility ($\chi = M/H$, T = 5–300 K) and heat capacity (C_p, 3–100 K) were measured on a Quantum Design – PPMS using the VSM and HC options, respectively. $\chi(T)$ was measured at a field of 10 kOe, and the Curie–Weiss law was fitted in the linear region (100–300 K) of the χ^{-1} *vs.* T plot.

Elemental analysis

Semiquantitative EDX analyses of the single crystals studied on a diffractometer were carried out in variable pressure mode using a Zeiss EVO® MA10 scanning electron microscope with CeO_2, Ag, and Ge as standards. The O/N-content was analyzed by the company Pascher (Remagen, Germany). A carrier hot gas extraction method was used after the pyrolysis of the sample in a graphite crucible followed by IR/thermal conductivity detection.

Electronic structure calculations

Electronic band structure calculations were performed with the WIEN2k program package[31] using density functional theory (DFT) within the full-potential LAPW+lo method and generalized gradient approximation (GGA) with 6 Ry separation energy between the core and valence states. The energy and charge convergence criteria were 10^{-5} Ry per cell and 10^{-4} e per cell, respectively. 48 Irreducible k-points were used with a plane wave cut-off of $R_{mt}K_{max}$ = 7.0. For detailed

Table 3 Anisotropic displacement parameters for $Ce_4Ag_3Ge_4O_{0.5}$ and $Ce_3Ag_4Ge_4$

Atom	U_{11}	U_{22}	U_{33}	U_{13}
$Ce_4Ag_3Ge_4O_{0.5}$				
Ce1	0.0095(2)	0.00838(19)	0.01133(19)	−0.0001(2)
Ce2	0.0103(2)	0.0096(2)	0.01059(19)	−0.0002(2)
Ce3	0.0092(2)	0.0080(2)	0.01294(19)	0.0010(2)
Ce4	0.0094(2)	0.0141(2)	0.01096(19)	−0.0005(2)
Ge1	0.0111(4)	0.0085(4)	0.0121(3)	−0.0017(3)
Ge2	0.0110(4)	0.0094(4)	0.0112(3)	−0.0005(3)
Ge3	0.0111(4)	0.0083(4)	0.0123(4)	0.0002(3)
Ge4	0.0112(4)	0.0096(4)	0.0223(4)	−0.0011(3)
Ag1	0.0179(3)	0.0132(3)	0.0143(3)	−0.0006(2)
Ag2	0.0210(3)	0.0116(3)	0.0131(3)	−0.0027(2)
Ag3	0.0141(3)	0.0126(3)	0.0160(3)	−0.0028(2)
O	0.023(6)	0.023(6)	0.028(6)	−0.006(5)
Atom	U_{11}	U_{22}	U_{33}	U_{12}
$Ce_3Ag_4Ge_4$				
Ce1	0.0090(4)	0.0085(5)	0.0099(4)	0.000
Ce2	0.0074(3)	0.0128(4)	0.0080(3)	0.000
Ag	0.0154(3)	0.0126(4)	0.0164(3)	−0.0042(2)
Ge1	0.0092(5)	0.0197(7)	0.0082(5)	0.000
Ge2	0.0089(5)	0.0098(6)	0.0119(6)	0.000

Table 4 Interatomic distances (pm), calculated with the powder lattice parameters in $Ce_4Ag_3Ge_4O_{0.5}$ and $Ce_3Ag_4Ge_4$. All distances of the first coordination spheres are listed

$Ce_4Ag_3Ge_4O_{0.5}$							
Ce1–Ge4	318.5(1) 2x	Ce2–Ge3	311.8(1) 2x	Ce3–Ge2	315.7(1) 2x	Ce4–Ge1	307.6(1)
Ce1–Ge2	322.3(1) 2x	Ce2–Ge4a	317.0(1) 2x	Ce3–Ge3	316.7(1) 2x	Ce4–Ge3	309.2(2)
Ce1–Ag2a	322.6(1) 2x	Ce2–Ge4b	317.8(1)	Ce3–Ge1	322.4(1) 2x	Ce4–Ge2	312.6(1) 2x
Ce1–Ge1	324.5(1) 2x	Ce2–Ag1a	342.5(1)	Ce3–Ag3a	323.1(1)	Ce4–Ag3	351.5(1) 2x
Ce1–Ag1	328.4(1)	Ce2–Ag1b	346.5(1) 2x	Ce3–Ag1	323.6(1) 2x	Ce4–Ag2	352.5(1) 2x
Ce1–Ag2b	350.2(1)	Ce2–Ag3	348.6(1)	Ce3–Ag2	325.5(1)	Ce4–Ce2	377.0(1) 2x
Ce1–Ce4	379.6(1)	Ce2–Ce4	377.0(1) 2x	Ce3–Ag3b	329.8(1) 2x		
						Ce1–O	237.0(10)
						Ce2–O	237.3(10)
						Ce4–O	243.2(4) 2x
						Ce1–O	237.0(10)
Ge1–Ge2	251.0(1)	Ge2–Ag2	276.3(1)	Ge3–Ag3a	273.1(1) 2x	Ge4–Ag1	268.3(1) 2x
Ge1–Ag2	262.7(1) 2x	Ge2–Ag3	279.0(2)	Ge3–Ag1	277.7(1)	Ge4–Ag2	288.1(1)
Ge1–Ag1	288.8(1)	Ge2–Ce4	312.6(1) 2x	Ge3–Ag3b	283.3(1)	Ge4–Ce2a	317.0(1) 2x
Ge1–Ce3	322.4(1) 2x	Ge2–Ce3	315.7(1) 2x	Ge3–Ce4	309.2(2)	Ge4–Ce2b	317.8(1)
Ge1–Ce1	224.5(1)	Ge2–Ce1	322.3(1) 2x	Ge3–Ce2	311.8(1) 2x	Ge4–Ce1	318.5(1) 2x
				Ge3–Ce3	316.7(1) 2x		
$Ce_3Ag_4Ge_4$							
Ce1–Ge2	319.3(1) 4x	Ce2–Aga	317.6(1) 4x	Ge1–Aga	272.3(1) 4x	Ge2–Ge2	257.0(2)
Ce1–Ge1	320.3(2) 2x	Ce2–Ge1	319.1(1) 2x	Ge1–Agb	278.4(1)	Ge2–Ag	263.9(1) 2x
Ce1–Ag	361.1(1) 8x	Ce2–Ge2	321.5(1) 4x	Ge1–Ce2	319.1(1) 2x	Ge2–Ce1	319.3(1) 2x
		Ce2–Agb	330.3(1) 2x	Ge1–Ce1	320.3(2)	Ge2–Ce2	321.5(1) 3x

descriptions see ref. 32 and 33. In order to achieve a better description of the localized Ce-4*f* states we have used the GGA+U approach including SIC (self-interaction correction) with an effective Hubbard U_{eff} of 7 eV.

Results and discussion

The crystal structure of $Ce_4Ag_3Ge_4O_{0.5}$ was solved on the basis of a single crystal structure determination revealing a new structure type. Fig. 1 presents a view along the *b* axis. The structure can be subdivided into two substructures, *i.e.* linear chains of oxygen-centred $[OCe_2Ce_{2/2}]$ tetrahedra, which are embedded in a three-dimensional network composed of $[CeAg_3Ge_4]$.

The structure refinement clearly revealed an occupancy of 52(2)% for the oxygen position. Careful analyses of the data set did not reveal any superstructure reflections and any diffuse scattering; the oxygen atoms statistically occupy the tetrahedral sites. The structural refinement without a half occupied oxygen position at the tetrahedral site resulted in remarkably higher residuals (*e.g.* R_1 = 0.0270 with oxygen and R_1 = 0.0340 without oxygen ($I > 2\sigma(I)$). The tetrahedra are made of the Ce1, Ce2, and Ce4 atoms at Ce–O distances ranging from 237 to 243 pm in excellent agreement with the Ce–O distance in the tetrahedral building units of CeMnSbO (239 pm)[34] and Ce_2AuP_2O (238–242 pm).[35] The structural motif of chains of corner-sharing tetrahedra is also known from the structures of Ca_3AlAs_3 [36,37] and Sm_3NS_3.[38,39]

The three-dimensional $[CeAg_3Ge_4]$ network has structural building units, which are well known from various rare earth-transition metal-silicides and germanides. All three crystallographically independent silver atoms have four germanium neighbours at Ag–Ge distances ranging from 263 to 289 pm slightly longer than the sum of the covalent radii of 256 pm.[40]

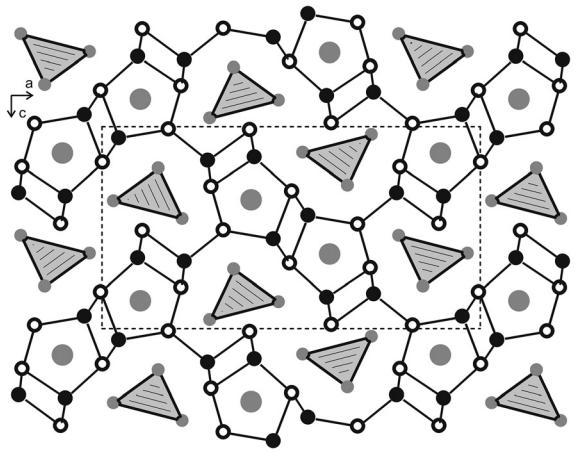

Fig. 1 Projection of the $Ce_4Ag_3Ge_4O_{0.5}$ structure onto the *ac* plane. Cerium, silver, and germanium atoms are represented as medium grey, black filled, and open circles, respectively. The three-dimensional $[CeAg_3Ge_4]$ network and the chains of corner-sharing oxygen centered $[OCe_2Ce_{2/2}]$ tetrahedra are emphasized.

Within this network, we observed various weak Ag–Ag contacts (319–340 pm Ag–Ag), slightly longer than the Ag–Ag distance in fcc silver (289 pm)[41] as well as typical d^{10}–d^{10} interactions.[42]

The $Ce_4Ag_3Ge_4O_{0.5}$ structure contains four crystallographically independent germanium sites. While the Ge3 and Ge4 atoms are isolated, the Ge1 and Ge2 atoms build Ge_2 dumbbells with a Ge1–Ge2 distance of 251 pm, a little bit longer than in elemental germanium (245 pm).[41] The substructure, built up from silver and germanium atoms, leaves slightly distorted pentagonal prismatic voids, which are filled with Ce3 atoms (Fig. 1). These prisms are condensed *via* Ag_2Ge_2 rhombs, a structural motif frequently observed in related intermetallic structures. It is worthwhile to note that similar structural features with almost similar interatomic distances were recently discovered in the $Gd_3Cu_4Ge_4$ type structure of $Ce_3Ag_4Ge_4$ (Fig. 2).[43] Interestingly, the phase $Ce_3Ag_4Ge_4$ was observed several times as a by-product during the various syntheses of $Ce_4Ag_3Ge_4O_{0.5}$. In contrast to the results of Szytuła *et al.*,[43] who presented neutron diffraction data on polycrystalline samples, the crystallinity of $Ce_3Ag_4Ge_4$, prepared under HP/HT conditions, allowed us to perform a single crystal structure determination with precise structural data (Tables 1 and 2). For a more detailed crystal chemical description of that structure type, refer to a publication on isotypic $Yb_3Pd_4Ge_4$.[44]

To examine the oxidation state of the cerium atoms in $Ce_4Ag_3Ge_4O_{0.5}$, magnetic measurements were performed. Fig. 3 shows the inverse magnetic susceptibility of $Ce_4Ag_3Ge_4O_{0.5}$.

We observed Curie–Weiss behavior above 100 K with an experimental magnetic moment of 2.42 μ_B per Ce atom, close to the value of 2.54 μ_B for the free Ce^{3+} ion, clearly indicating trivalent cerium in $Ce_4Ag_3Ge_4O_{0.5}$.[45] The negative Weiss constant of −8.6 K is indicative of antiferromagnetic interactions in the paramagnetic range. Magnetic ordering at 3.2 K was evident from low-temperature specific heat data (Fig. 3).

The elemental analysis of $Ce_4Ag_3Ge_4O_{0.5}$ by EDX analysis of the elements Ce, Ag, and Ge revealed: Ce: 47% (47.4%) (theoretical values in brackets); Ag: 27% (27.4%); Ge: 26% (24.6%). To detect the small oxygen content and a possible nitrogen contamination, the O/N-content was analyzed by an IR/thermal conductivity detection. The amount of oxygen came to a value

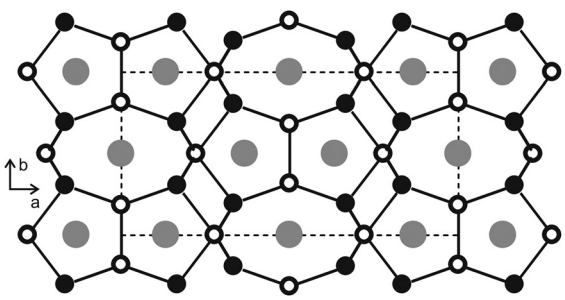

Fig. 2 Projection of the $Ce_3Ag_4Ge_4$ structure onto the *ab* plane. Cerium, silver, and germanium atoms are drawn as medium grey, black filled, and open circles, respectively. The three-dimensional $[Ag_4Ge_4]$ network is emphasized.

Published on 12 September 2013.

This journal is © The Royal Society of Chemistry 2013

Published on 12 September 2013.

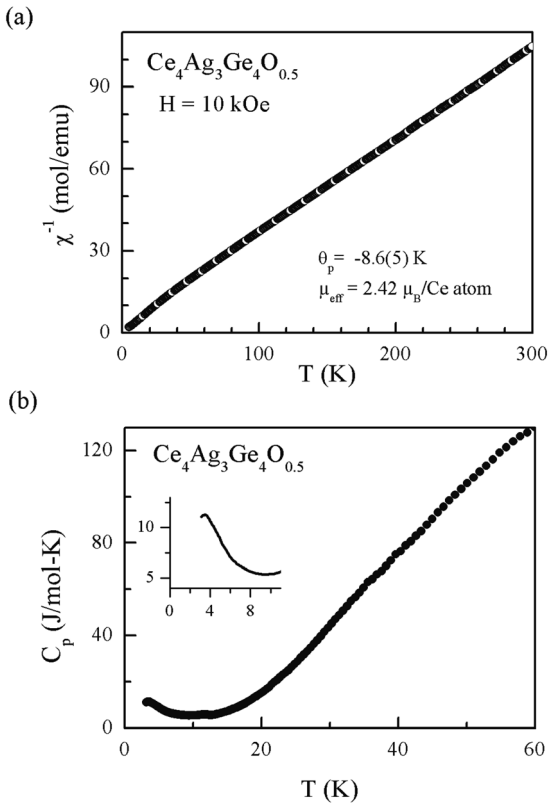

Fig. 3 A plot of χ^{-1} *vs.* T is shown in (a). The C_p as a function of T is shown in (b). The inset shows the low temperature (<10 K) features on an expanded scale. The onset of magnetic ordering below 3.2 K is clearly visualized in the inset.

of 0.65 %, which fits well to the expected theoretical value of 0.68 %. Only traces of nitrogen were detected.

Considering the trivalent and monovalent oxidation states for the cerium and silver atoms, closed-shell Ge^{4-} and Ge_2^{6-} dumb-bells, and a half occupied oxygen site, we obtain the following ionic formula splitting: $(4Ce^{3+})^{12+}(3Ag^{+})^{3+}(2Ge^{4-})^{8-}$-$Ge_2^{6-}(1/2O^{2-})^{-}$. Nevertheless, $Ce_4Ag_3Ge_4O_{0.5}$ should be regarded as a metallic compound, possessing an ionic $[OCe_2Ce_{2/2}]$-strand inside a metallic matrix. A similar bonding pattern occurs in a variety of subnitrides, *e.g.* isolated Ba_6N octahedra in a sodium matrix of $Na_{16}Ba_6N$.[46,47]

To substantiate the findings regarding the metallic state and the magnetic properties, we performed DFT band structure calculations of idealized $Ce_4Ag_3Ge_4O$ (full occupancy of the O-site) using the full potential LAPW method.

The calculations converged in a magnetic ground state with 0.97 unpaired electrons per cerium in excellent agreement with the experimental data, and confirm the trivalent state of cerium. Since the detailed magnetic spin structure is unknown, we confined our calculations to a ferromagnetic model. The DOS shown in Fig. 4 reveals a metallic state without contributions of the Ce-4f states, which are pushed away from E_F by the on-site Coulomb repulsion. The 7 eV gap in the 4*f* states depends on the choice of U_{eff} which has not been optimized. The states at the Fermi-energy are dominated

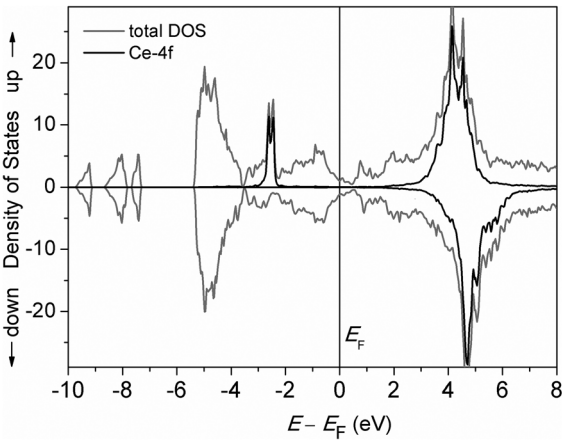

Fig. 4 Spin polarized density of states of $Ce_4Ag_3Ge_4O$. Grey: total DOS, black: contributions of the Ce-4*f* states. An effective Hubbard U_{eff} of 7 eV was applied to the Ce-4*f* shell. The Fermi level is taken at the energy of zero.

by Ge- and to a smaller extent by Ag-contributions; thus the Ag_3Ge_4-network is the base of the metallic property. The Ag-4d-states are around −5 eV and relatively broad, probably because of the relatively short Ag–Ag distances that allow weak d^{10}–d^{10} interactions.

Temperature dependent X-ray powder investigations under argon revealed the stability of $Ce_4Ag_3Ge_4O_{0.5}$ up to a temperature of 650 °C (Fig. 5). Exceeding this temperature, $Ce_4Ag_3Ge_4O_{0.5}$ decomposed into $Ce_3Ag_4Ge_4$. The decomposition was completed at 800 °C, remaining stable after cooling down to room temperature.

Finally we present the comparison of the $Ce_4Ag_3Ge_4O_{0.5}$ structure with the large family of pnictide oxide superconductors.[23,24] This fascinating field of solid state chemistry is dominated by the many tetragonal phases, which are built up from polycationic and polyanionic layers. The most prominent phase is LaFeAsO[48] which becomes superconducting upon fluorine doping on the oxygen site. The large majority of the ZrCuSiAs type and related pnictide oxides exclusively show layers of condensed, edge-sharing ORE_4 tetrahedra in the polycationic part.[49,50] $Ce_4Ag_3Ge_4O_{0.5}$ (Fig. 1) and Ce_2AuP_2O[35] (Fig. 6) are first examples with one-dimensional polycationic

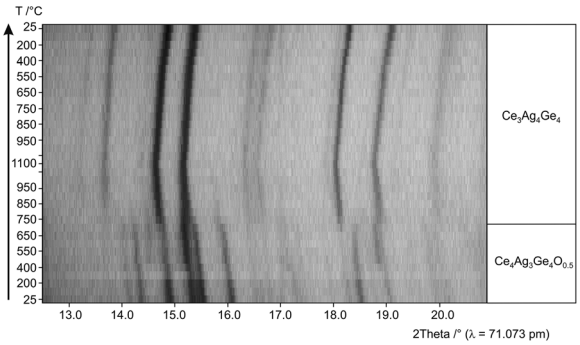

Fig. 5 Temperature-programmed X-ray powder patterns following the decomposition reaction of the metastable high-pressure phase $Ce_4Ag_3Ge_4O_{0.5}$.

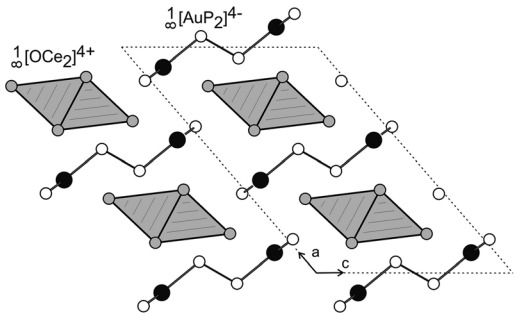

Fig. 6 View of the Ce_2AuP_2O structure along the monoclinic axis. Cerium, gold, and phosphorus atoms are represented as medium grey, black filled, and open circles, respectively. The strands of edge-sharing $OCe_{4/2}$ tetrahedra and the $[AuP_2]$ polyanions are emphasized.

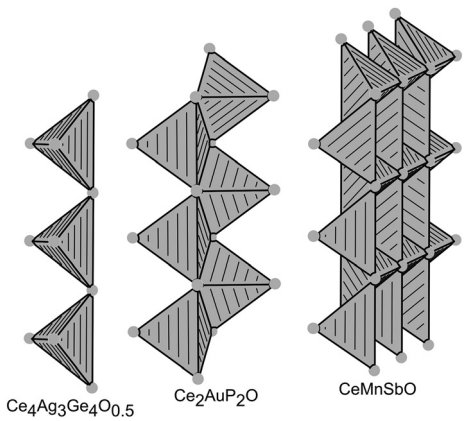

Fig. 7 The substructures of condensed OCe_4 tetrahedra in $Ce_4Ag_3Ge_4O_{0.5}$, Ce_2AuP_2O, and CeMnSbO.

units. The surrounding polyanionic part is three-dimensional in $Ce_4Ag_3Ge_4O_{0.5}$ but consists of isolated $[AuP_2]^{4-}$ polyanions in Ce_2AuP_2O (Fig. 6).[35]

Fig. 7 summarizes the polycationic substructures in $Ce_4Ag_3Ge_4O_{0.5}$, Ce_2AuP_2O,[35] and CeMnSbO.[34] The OCe_4 tetrahedra share common corners in the structure of $Ce_4Ag_3Ge_4O_{0.5}$. This motif is duplicated in Ce_2AuP_2O, where condensation of a second chain leads to edge-sharing tetrahedra. Both of these motifs are one-dimensional. In CeMnSbO,[34] we observe the layer, which results from condensation of the rows observed in Ce_2AuP_2O. Although the tetragonal phases are by far the majority in the family of pnictide oxide superconductors, we can still expect interesting new motifs in this exciting field of solids as demonstrated by the present HP–HT route.

Conclusions

We reported on the first example of the oxidation of an intermetallic phase under high-pressure/high-temperature conditions, leading to a new germanide oxide with the composition $Ce_4Ag_3Ge_4O_{0.5}$. The structure can be subdivided into two substructures, *i.e.* linear chains of oxygen-centred $[OCe_2Ce_{2/2}]$ tetrahedra, which are embedded in a three-dimensional network composed of $[CeAg_3Ge_4]$. Curie–Weiss behavior above 100 K with an experimental magnetic moment of 2.42 μ_B per Ce atom clearly indicated trivalent cerium. DFT band structure calculations resulted in metallic properties and in a magnetic ground state, compatible with one unpaired 4*f*-electron per cerium.

Acknowledgements

We thank the Deutsche Forschungsgemeinschaft (HU 966/4-1 and PO 573/10-1) for generous support, Dr P. Mayer for collecting the single crystal data, T. Miller for the temperature programmed XRD-data, and Prof. Dr W. Schnick (LMU München) for the continuous support of these investigations. S. Rayaprol is indebted to the AvH foundation for a research stipend and H. Huppertz to the Fonds der Chemischen Industrie for financial support.

Notes and references

1 R. Demchyna, S. Leoni, H. Rosner and U. Schwarz, *Z. Kristallogr.*, 2006, **221**, 420.
2 J. F. Riecken, G. Heymann, T. Soltner, R.-D. Hoffmann, H. Huppertz, D. Johrendt and R. Pöttgen, *Z. Naturforsch., B: Chem. Sci.*, 2005, **60**, 821.
3 G. Heymann, S. Rayaprol, J. F. Riecken, R.-D. Hoffmann, U. C. Rodewald, H. Huppertz and R. Pöttgen, *Solid State Sci.*, 2006, **8**, 1258.
4 J. F. Riecken, U. C. Rodewald, G. Heymann, S. Rayaprol, H. Huppertz, R.-D. Hoffmann and R. Pöttgen, *Z. Naturforsch. B: Chem. Sci.*, 2006, **61**, 1477.
5 G. Heymann, J. F. Riecken, S. Rayaprol, S. Christian, R. Pöttgen and H. Huppertz, *Z. Anorg. Allg. Chem.*, 2006, **633**, 77.
6 R. Hoppe and H. J. Röhrborn, *Naturwissenschaften*, 1961, **12**, 453.
7 R. Hoppe and H. J. Röhrborn, *Z. Anorg. Allg. Chem.*, 1964, **327**, 199.
8 R. Hoppe, *J. Solid State Chem.*, 1986, **65**, 127.
9 H.-D. Wasel-Nielen and R. Hoppe, *Z. Anorg. Allg. Chem.*, 1968, **36**, 359.
10 P. J. Yvon, R. B. Schwarz, C. B. Pierce, L. Bernadez, A. Conners and R. Meisenheimer, *Phys. Rev. B: Condens. Matter*, 1989, **39**, 6690.
11 W. Schauerte, H.-U. Schuster, N. Knauf and R. Müller, *Z. Anorg. Allg. Chem.*, 1992, **616**, 186.
12 B. Cogel and H.-U. Schuster, *Z. Anorg. Allg. Chem.*, 1993, **619**, 1765.
13 H.-U. Schuster and J. Wittrock, *J. Therm. Anal.*, 1993, **39**, 1397.
14 A. Panahandeh and W. Jung, *Z. Anorg. Allg. Chem.*, 2003, **629**, 1651.

Published on 12 September 2013.

 This journal is © The Royal Society of Chemistry 2013

15 M. P. Dariel and M. R. Pickus, *J. Less-Common Met.*, 1976, **50**, 125.
16 R. Mackay and H. F. Franzen, *J. Alloys Compd.*, 1992, **186**, L7.
17 H. Nowotny, B. Lux and H. Kudielka, *Monatsh. Chem.*, 1956, **87**, 447.
18 E. Parthé, *Powder Metal. Bull.*, 1957, **8**, 23.
19 E. Parthé and J. T. Norton, *Acta Crystallogr.*, 1958, **11**, 14.
20 V. K. Pecharskii, K. A. Gschneidner Jr., O. I. Bodak and A. S. Protsyk, *J. Less-Common Met.*, 1991, **168**, 257.
21 E. Cordruwisch, D. Kaczorowski, A. Saccone, P. Rogl and R. Ferro, *J. Phase Equilib.*, 1999, **20**, 407.
22 B. J. Gibson, R. Pöttgen and R. K. Kremer, *Physica B: Condens. Matter*, 2000, **276–278**, 734.
23 D. C. Johnston, *Adv. Phys.*, 2010, **59**, 803–1061.
24 D. Johrendt, H. Hosono, R.-D. Hoffmann and R. Pöttgen, *Z. Kristallogr.*, 2011, **226**, 435–446.
25 H. Huppertz, *Z. Kristallogr.*, 2004, **219**, 330.
26 G. M. Sheldrick, *SHELXS-97, Program for the Solution of Crystal Structures*, University of Göttingen, Göttingen (Germany), 1997.
27 G. M. Sheldrick, *Acta Crystallogr., Sect. A: Fundam. Crystallogr.*, 1990, **46**, 467.
28 G. M. Sheldrick, *Shelxl-97, Program for the Refinement of Crystal Structures*, University of Göttingen, Göttingen (Germany), 1997.
29 G. M. Sheldrick, *Acta Crystallogr., Sect. A: Fundam. Crystallogr.*, 2008, **64**, 112.
30 Z. Otwinowski and W. Minor, *Methods Enzymol.*, 1997, **276**, 307.
31 P. Blaha, K. Schwarz, G. K. H. Madsen, D. Kvasnicka and J. Luitz, *Wien2k – an augmented plane wave+local orbitals program for calculating crystal properties*, Wien, 2001.
32 K. Schwarz and P. Blaha, *Comput. Mater. Sci.*, 2003, **28**, 259.
33 D. J. Singh and L. Nordstrom, *Planewaves, Pseudopotentials and the LAPW Method*, Springer, New York, 2006.
34 I. Schellenberg, T. Nilges and R. Pöttgen, *Z. Naturforsch., B: Chem. Sci.*, 2008, **63**, 834.
35 T. Bartsch, T. Wiegand, J. Ren, H. Eckert, D. Johrendt, O. Niehaus, M. Eul and R. Pöttgen, *Inorg. Chem.*, 2013, **52**, 2094.
36 G. Cordier and H. Schäfer, *Angew. Chem., Int. Ed. Engl.*, 1981, **93**, 474.
37 G. Cordier, G. Savelsberg and H. Schäfer, *Z. Naturforsch., B: Anorg. Chem. Org. Chem.*, 1982, **37**, 975.
38 F. Lissner and T. Schleid, *Z. Anorg. Allg. Chem.*, 1993, **619**, 1771.
39 T. Schleid, *Eur. J. Solid State Inorg. Chem.*, 1996, **33**, 227.
40 J. Emsley, *The Elements*, Oxford University Press, Oxford (UK), 1999.
41 J. Donohue, *The Structures of the Elements*, Wiley, New York (USA), 1974.
42 M. Jansen, *Angew. Chem., Int. Ed. Engl.*, 1987, **99**, 1136.
43 A. Szytuła, D. Kaczorowski, S. Baran, J. Hernández-Velasco, B. Penc, N. Stüßer, E. Wawrzyńska and K. Gofryk, *Intermetallics*, 2006, **14**, 702.
44 D. Niepmann, Yu. M. Prots, R. Pöttgen and W. Jeitschko, *J. Solid State Chem.*, 2000, **154**, 329.
45 H. Lueken, *Magnetochemie*, Teubner, Stuttgart, 1999.
46 G. J. Snyder and A. Simon, *Angew. Chem., Int. Ed. Engl.*, 1994, **106**, 713.
47 A. Simon, *Coord. Chem. Rev.*, 1997, **163**, 253.
48 Y. Kamihara, T. Watanabe, M. Hirano and H. Hosono, *J. Am. Chem. Soc.*, 2008, **130**, 3296.
49 D. Johrendt and R. Pöttgen, *Angew. Chem., Int. Ed.*, 2008, **47**, 4782.
50 T. Ozawa and S. M. Kauzlarich, *Sci. Technol. Adv. Mater.*, 2008, **9**, 033003.

Published on 12 September 2013.